Preliminary double-difference relocation earthquake catalogue for southwestern Yukon centred along the Denali fault zone

Katherine Biegel*, Jeremy Gosselin and Jan Dettmer
Department of Geoscience, University of Calgary, Calgary, Alberta, Canada

Biegel, K., Gosselin, J. and Dettmer, J., 2023. Preliminary double-difference relocation earthquake catalogue for southwestern Yukon centred along the Denali fault zone. *In:* Yukon Exploration and Geology 2022, K.E. MacFarlane (ed.), Yukon Geological Survey, p. 1–18, plus digital appendices.

Abstract

Southwestern Yukon is a seismically active zone of crustal deformation including multiple large, dextral strike-slip fault systems with overlapping activity. In this study, we perform double-difference relocation to the USGS earthquake catalogue for this region to produce a relocated catalogue of 5536 seismic events above magnitude 1.5 from 2010–2021. The relocated catalogue demonstrates better spatial resolution of linear features and the removal of grid location artifacts in depth. The relocated catalogue has smaller travel time residuals and smaller residual standard deviations showing that the new catalogue has improved absolute locations. From bootstrapping, we estimate the location uncertainties for the relocated events to be on the order of 1.2–2.4 km in the horizontal direction and 1.5–2.1 km in the vertical direction. From the relocated events, we interpret new faults including a fault connecting the Totschunda and Denali faults, a connector fault between the Totschunda-Duke River fault system and the Fairweather fault, and multiple smaller faults connecting the Fairweather and Denali faults. The significantly reduced uncertainty in depth also permits constraining the seismicity predominantly to the uppermost 10 km of the crust.

* katherine.biegel@ucalgary.ca

Introduction

Regional tectonic setting

Southwestern Yukon is a zone of active tectonic deformation. The Yakutat block, a tectonic microplate, is obliquely colliding with the North American Plate. The microplate bridges the transition zone from the Aleutian Trench, where the Pacific Plate is subducting under the North American Plate, to the Fairweather/ Queen Charlotte fault, the dextral transform zone that delineates the boundary between the Pacific and North American plates. Current subduction of the Yakutat block is occurring at a rate of 2 mm/yr (Lundgren et *al.*, 1995) with crustal deformation focused in the St. Elias Mountain Range. The Pacific Plate is moving at a rate of 5.7 cm/yr to the northwest (Fig. 1) relative to the North American Plate (DeMets et *al.*, 1990).

Southwestern Yukon has several major dextral crustal strike-slip fault systems including the Chugach-St. Elias fault, Fairweather fault, Denali fault and the Teslin fault farther to the east (Fig. 1). Most regional deformation occurs in the St. Elias region along the Chugach–St. Elias fault or the Fairweather fault. While this region in the St. Elias Mountains is dominated by thrust faulting,

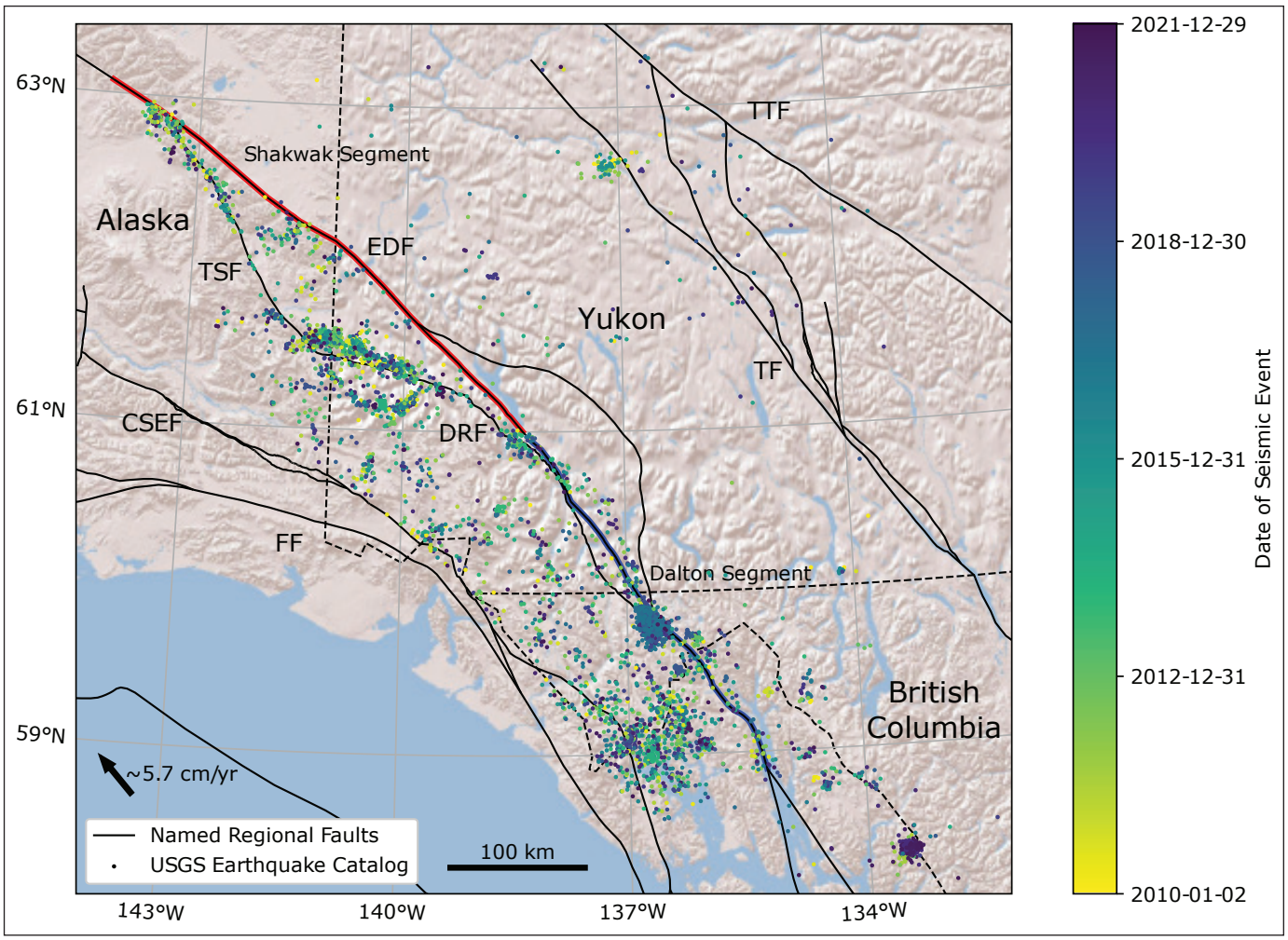

Figure 1. *Seismic events of interest. Epicentral locations (dots) of intraplate seismic events over magnitude 1.5 occurring between Jan. 2010 and Dec. 2021 (colour scale) as defined by the USGS earthquake catalogue. Mapped major regional faults (black lines; after Yukon Geological Survey, 2020) are indicated with major faults of interest labeled including the Tintina fault (TTF), Teslin fault (TF), Eastern Denali fault (EDF), Totschunda fault (TSF), Duke River fault (DRF), Chugach-St. Elias fault (CSEF), and Fairweather fault (FF). Coloured lines indicate subdivisions of the Eastern Denali fault including the Shakwak segment (red line; Grantz, 1966) and the Dalton Segment (blue line; Lanphere, 1977). Political boundaries are denoted by a dashed line.*

the Fairweather fault is a predominately dextral strike-slip fault with slip estimated between 36.6 and 58 mm/yr (Plafker *et al.*, 1978; Fletcher and Freymueller, 2003; Elliott *et al.*, 2010). The St. Elias Mountains are an accretionary mountain range consisting of multiple terranes that were juxtaposed during Yakutat block subduction. The St. Elias Mountains are bound on the eastern side by the Denali fault. Most current crustal seismicity in the region occurs in the zone of deformation between the Fairweather and Denali faults.

The Denali fault is a major dextral, strike-slip fault zone that stretches from central Alaska to British Columbia through southwestern Yukon. Historically there is approximately 400 to 480 km of accumulated slip along the Denali fault (Lowey, 1998; Waldien *et al.*, 2021). Grantz (1966) subdivided the Denali fault into three segments: the Western Denali fault in west-central Alaska, the Central Denali fault in eastern Alaska, and the Eastern Denali fault in southwestern Yukon (Fig. 2). The fault was most active during the Holocene, particularly along the McKinley segment of its central portion and along the Totschunda fault to the south (Lanphere, 1977). The last major earthquake in this area was the 2002 magnitude (M) 7.9 Denali earthquake, a slip-partitioned event, rupturing portions of the Central Denali fault before rupturing the Totschunda fault (Eberhart-Phillips *et al.*, 2003). Slip estimates along the Central Denali fault are ~12.1 mm/yr (Matmon *et al.*, 2006).

The Eastern Denali fault in Yukon is further divided into the Shakwak and Dalton sections (Grantz, 1966; Lanphere, 1977). The Shakwak section of the Denali fault extends from the junction with the Totschunda fault to the Duke River fault (Fig. 1). The Shakwak section is less active than the Central Denali fault in Alaska. Previous studies place movement on the Shakwak section in the range of 5 to 8.4 mm/yr (Matmon *et al.*, 2006; Seitz *et al.*, 2008; Kalbas *et al.*, 2008). The Dalton section of the Denali fault extends from the Duke River fault to the Chatham Strait (Fig. 1) and

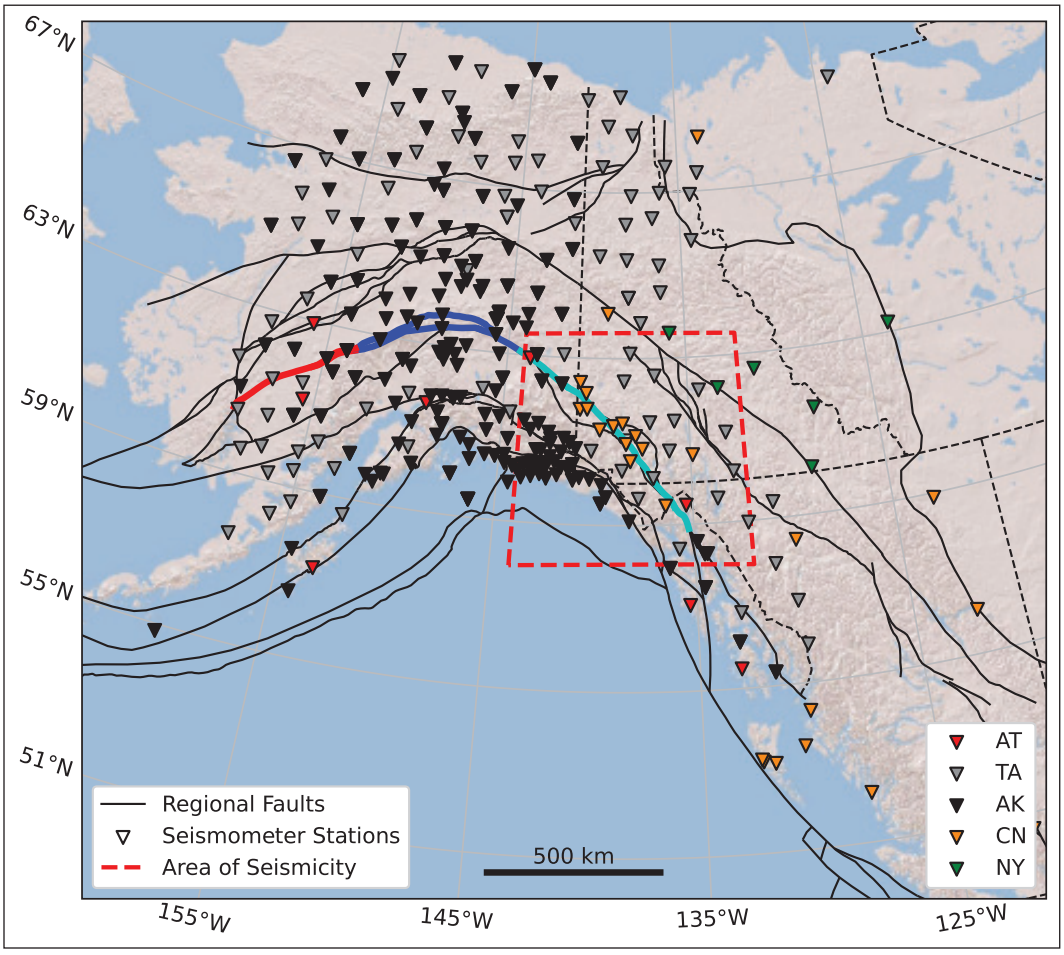

Figure 2. *Locations of seismic stations (triangles) in Alaska and Canada with at least 1 pick arrival for seismicity (Fig. 1) occurring within the study area of seismicity (red dashed box). Seismic networks are denoted by the colour and include the Alaska Tsunami Network (AT; red), the Transportable Array (TA; gray), the Alaska Regional Network (AK; black), the Canadian National Network (CN; orange), and the Yukon-Northwest Network (NY; green). Major regional faults (black lines) are also shown (after Yukon Geological Survey, 2020). The major subdivisions of the Denali fault (Grantz, 1966) are denoted by the coloured line sections: the Western Denali fault (red), the Central Denali fault (blue) and the Eastern Denali fault (cyan).*

has the smallest slip rate of 1.0–2.5 mm/yr as well as approximately 1.5 mm/yr of contraction (Plafker et *al*., 1994; Kalbas et *al*., 2008; Leonard et *al*., 2008; Elliott et *al*., 2010). Prior studies suggest that the Eastern Denali fault serves as a regional stress boundary while active deformation occurs on other fault systems such as the Duke River fault (Choi et *al*., 2021).

Relative seismic event location and relocation

Double-difference (DD) relocation is a relative earthquake location methodology that focuses on relative precision of clusters of earthquakes, rather than the absolute location of individual events. Relative location methods can generally be categorized by how events are paired or related to one another. Parent event approaches (Ito, 1985; Scherbaum and Wendler, 1986; VanDecar and Crosson, 1990) define larger, well-located events as the "parent" events and locate surrounding seismicity ("child" events) in relation to these. Joint hypocentre methods rely on the concept of the earthquake doublet (Fréchet, 1985), for events of similar source location and mechanism. For these methods (Douglas, 1967; Dodge et *al*., 1995; Waldhauser and Ellsworth, 2000), the location of the doublet is defined by the centroid or joint hypocentre for the pair. Many relative location methods can be used to define an initial seismic event catalogue or as a relocation method to further refine catalogue precision for an existing seismic event catalogue.

As a widely applied joint-hypocentre (doublet) relocation method, DD relocation is a method of defining a relocation catalogue from differential travel time pairs. Pairs of differential travel times come from either an event-pair (a pair of events measured at a common station) or a station-pair (a common event measured at a pair of stations). The most widely applied DD method is event-pair DD relocation (Waldhauser and Ellsworth, 2000) which can be applied across seismic event scales from microseismic studies (Castellanos and Van der Baan, 2013) to regional tectonic studies (Schaff et al., 2002; Waldhauser et *al*., 2004; Waldhauser and Schaff, 2008). This method can be used to recover absolute event locations (Menke and Schaff, 2004) and reduces the effect of velocity model errors on the relocation. However, the method does not completely remove reliance on the choice of velocity model and a poorly chosen velocity model can lead to bias in the final solution (Wolfe, 2002; Michelini and Lomax, 2004). The reciprocal solution, station-pair DD relocation, has been applied to non-volcanic tremors as an absolute location method (Zhang et *al*., 2010). Finally, the double-pair DD method, combining both event and station-pair information, has also been shown to improve both relative and absolute event locations (Guo and Zhang, 2016). The double-pair method has been applied at regional tectonic scales (Guo et *al*., 2017; Li et *al*., 2018; Ogwari et *al*., 2018; Share et *al*., 2021).

Study motivation

This study is part of a larger, multi-year investigation of the geothermal energy potential and natural hazards of major fault zones in southern Yukon. Previous studies have suggested that southern Yukon may have geothermal resources indicated by shallow Curie point depths (Li et *al*., 2017), large regional fault systems, and the surface manifestations of warm water circulation such as hot springs (Langevin et *al*., 2020).

In this study, we present a relocated earthquake catalogue for seismicity in southwestern Yukon (Fig. 1) using the event-pair DD relocation method. Our results further refine event locations and improve cluster location precision to help highlight existing fault structures. The relocated catalogue is provided as a geophysical dataset as part of this report (Appendix A). This result will allow for a refined regional tectonic interpretation of active seismicity leading to further studies of source mechanisms and regional stress (Gosselin et *al*., 2023).

Methods

Double-difference relocation

The DD relocation begins with the linearization of the travel time, *t*, equation (Geiger, 1910) for earthquake i at station *k*,

$$r_k^i = \frac{\partial t_k^i}{\partial \boldsymbol{m}} \Delta \boldsymbol{m}^i + \Delta\tau_i + s_k \qquad (1)$$

where r_k^i is the travel time residual (t^{obs}-t^{cal}), $\Delta\mathbf{m}^i$ are model parameter perturbations (Δx^i, Δy^i, Δz^i), $\Delta\tau_i$ is the origin time correction, and s_k is the station correction.

For a catalogue of events observed with a seismic network, differential residuals can be taken for pairs of travel time residuals. This differential residual is known as a *double-difference*.

The event-pair DD (Waldhauser and Ellsworth, 2000) is defined for an event pair, events *i* and *j*, at a common station, *k*,

$$dr_k^{ij} = \left(\frac{\partial t_k^i}{\partial \boldsymbol{m}} \Delta \boldsymbol{m}^i + \Delta\tau_i\right) - \left(\frac{\partial t_k^j}{\partial \boldsymbol{m}} \Delta \boldsymbol{m}^j + \Delta\tau_j\right) \quad (2)$$

where dr_k^{ij} is the differential residual, $(t_k^i - t_k^j)^{obs} - (t_k^i - t_k^j)^{cal}$, and model perturbations, $\Delta\boldsymbol{m}^i$ and $\Delta\boldsymbol{m}^j$, are defined for the two events. The station correction term cancels.

Inversion methods and data weighting

Over an entire catalogue of pairs, Eq. (2) can be characterized by the linear form

$$\boldsymbol{WGm} = \boldsymbol{Wd} \quad (3)$$

where vector $\boldsymbol{d}$ are the data (DD residuals), vector $\boldsymbol{m}$ contains model parameters (4 perturbations per seismic event), $\boldsymbol{G}$ is a matrix of partial time derivatives with respect to the model parameters, and $\boldsymbol{W}$ is a diagonal matrix containing data weights.

For the relocation problem considered here, the most appropriate method for solving for $\boldsymbol{m}$ is by iterative linear least-squares (Paige and Saunders, 1982). The iterative least-squares method requires a regularization or damping parameter, λ, to minimize DD residuals over the system

$$\begin{bmatrix} \boldsymbol{WG} \\ \lambda I \end{bmatrix} \boldsymbol{m} = \begin{bmatrix} \boldsymbol{Wd} \\ 0 \end{bmatrix} \quad (4)$$

We employ damping parameter selection by an automated L-curve criterion test (Aster *et al.*, 2018).

A priori data weights are based on catalogue pick quality and cross-correlation coefficients. Data weights are recalculated for each iteration of the inversion until the solution reaches stability. Due to the Gaussian error assumption in the linear least-square method, large residuals are down-weighted using bi-weighting (Mosteller and Tukey, 1977).

Using a method similar to Waldhauser and Ellsworth (2000), we assess relative location error estimates using a statistical resampling bootstrap approach (Billings, 1994; Shearer, 1997). For error estimation, we resample the differential-time data by drawing random samples with replacement from the observed residual distribution of the relocation catalogue. We relocate the catalogue using these resampled data as the starting catalogue, incorporating noise into the relocations. Resampling and relocation are repeated 250 times with the cumulative results allowing for estimation of the relocation catalogue uncertainty.

Data set

Earthquake catalogue

For this study, we have identified 6010 crustal seismic events from the USGS catalogue (Fig. 1). This catalogue includes all seismicity of magnitude >1.5 and occurring between 2010 and 2021 in the study area. Our catalogue is limited by the installation date of broadband seismic stations in Yukon which occurred in 2010 and effectively reduced the magnitude of completeness from ~3 to ~1 in some regions of Yukon (Meighan *et al.*, 2013). Our catalogue is also limited by the number of phase arrival observations for each event. As we solve for eight model parameters per event pair, event pairs require a minimum of eight shared observations per pair to become an evenly-determined problem. We have therefore limited the minimum magnitude of 1.5 based on the number of phase arrivals per event. Due to our interest in intraplate crustal seismicity, events occurring in proximity of the plate boundary or at depths greater than 30 km were removed from the initial catalogue.

The events of the starting catalogue were observed at 359 seismic stations (Fig. 2) in Alaska and Canada. These stations are part of the International Federation of Digital Seismograph Networks (FDSN) and include parts of the Alaska Tsunami (AT) Seismic Network, the USArray Transportable Array (TA), the Alaska Regional Network (AK), the Canadian National (CN)

Seismograph Network, and the Yukon–Northwest (NY) Seismic Network. Not all stations are temporally available for the entirety of this dataset. The AT, AK, CN, and NY are permanent networks. Most stations within these networks were operating throughout the entirety of the catalogue duration. The TA was a dense temporary station deployment that began in Alaska and parts of Yukon in 2014 and ended in 2021 (Busby and Aderhold, 2020). While not permanent as part of the TA, some of the temporary stations used in the TA deployment were transitioned to permanent stations as part of the AT, AK, and CN networks. Most of the TA stations in Yukon were removed during the 2020/2021 field seasons.

For this catalogue, the USGS identifies 140 186 phase arrivals including 100 265 P arrivals and 39 321 S arrivals. These catalogue arrivals are used as the starting measurements for calculating differential time catalogues.

Event pairing

Event-pairs are required for the calculation of differential time measurements. In this case, we limit event-pairs by the inter-event separation of 12.5 km and to a minimum of 8 common stations for shared measurements. Figure 3 shows the event-pairs included in the differential time catalogues. There were 30 542 event-pairs defined for the 6010 events. The average inter-event distance between event pairs is 4.094 km.

Differential time catalogues

For DD relocation, we develop two differential time (DT) catalogues: one from pick arrivals and one from waveform cross-correlations for each method of relocation. The DT catalogues from pick arrivals are calculated from travel time differences for event-pairs while the cross-correlation catalogues are calculated from up-sampled waveform cross-correlations centred on pick arrivals. This cross-correlation further refines

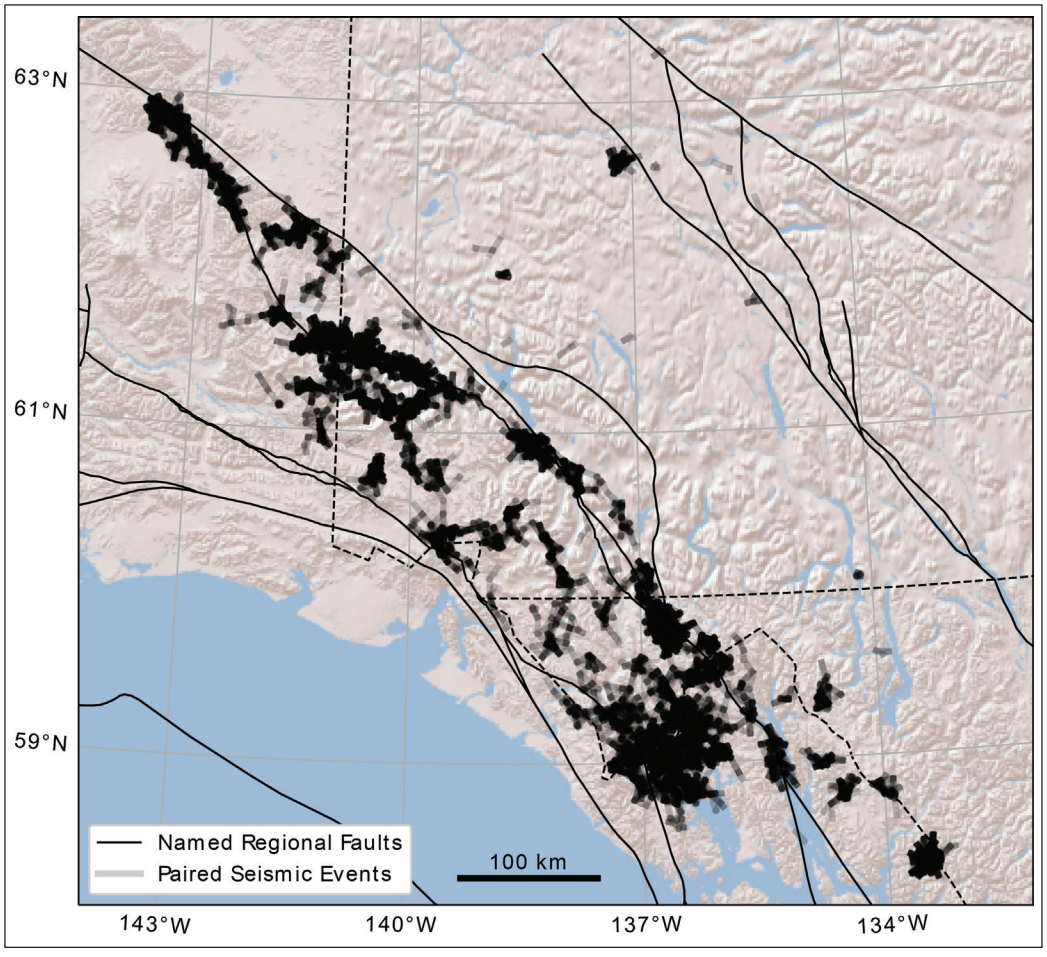

Figure 3. *Density of event-pairs over the study area. Event-pairs are plotted as transparent lines between paired events – darker areas indicate denser spatial coverage of event-pairing.*

the precision of catalogue picks to the onset of waveform similarities and leads to a more precise DT. Cross-correlations must have a correlation coefficient of 0.8 to be included in the cross-correlation DT catalogue.

For the event-pair DD relocations, the DT phase arrival catalogues include 320 028 P wave DTs and 120 600 S wave DTs. The event-pair DD cross-correlation DT catalogue includes 235 724 P wave DTs and 377 504 S wave DTs.

Results and preliminary interpretation

Event-pair relocation catalogue

Using the event-pair DD method, we relocated 5536 events (92% of the USGS catalogue). The full relocation catalogue is shown in Figure 4. where six areas of interest, labeled AA' to FF', are identified. From this relocation catalogue, we find improved spatial linearization of seismicity as well as the removal of grid artifacts from catalogue locations, particularly in depth.

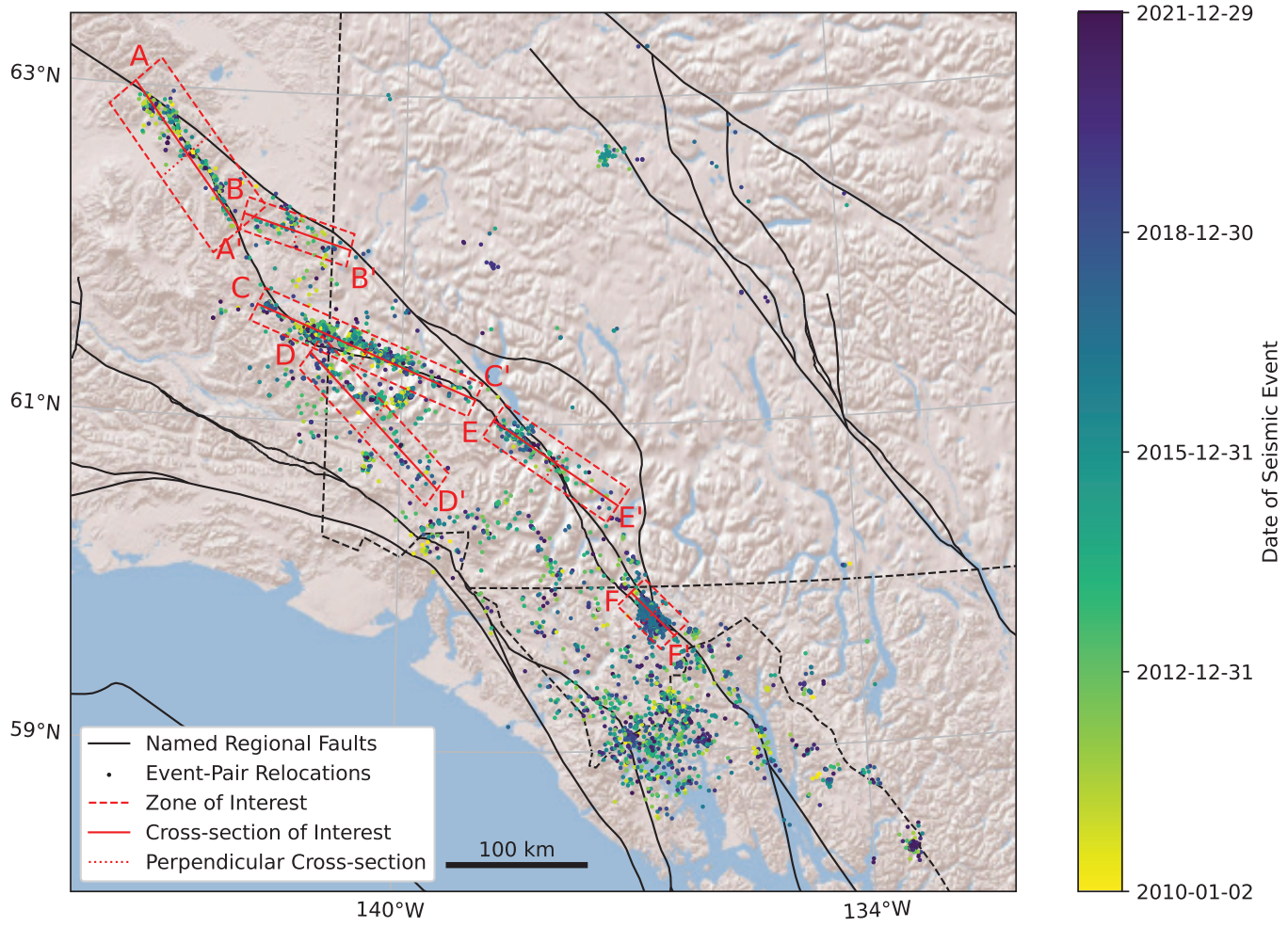

Figure 4. *Event-pair relocations (dots) coloured by date with 6 zones of interest (shown in red). The zones of interest are AA' (Totschunda fault seismicity), BB' (seismicity between the Totschunda and Denali faults), CC' (Duke River fault seismicity), DD' (Connector fault Seismicity), EE' (seismicity south of Kluane Lake crosscutting the Denali fault), and FF' (2017 St. Elias sequence aftershock events). Each zone of interest includes the cross section of interest (solid line), the perpendicular cross section (dotted line), and the included seismicity (dashed box).*

The cross section AA' contains 239 events occurring on the Totschunda fault (Fig. 5). The majority of the seismicity here occurs along the segment of the Totschunda fault that ruptured during the 2002 M 7.9 Denali earthquake. Depth cross sections AA' and aa' (Fig. 5) show that event depths are predominantly <15 km. Along the main cross section (AA'), we see two NW–SE trends of decreasing depths from 0 to 75 km and 100 to 150 km.

Zone BB' (Fig. 6), containing only 76 events, is the smallest highlighted feature. It is a feature running parallel to the Duke River fault to the south and connecting the Totschunda and Denali faults. From the depth cross sections for both BB' and bb' (Fig. 6), the relocated event depths in this zone are 5 to 12 km. We interpret this feature as an active fault that connects the Totschunda and Denali faults. This fault could release stress due to rotation of the inter-fault region bounded by the Totschunda, Duke River and Denali faults.

Figure 7 shows 968 events in Zone CC', including events in proximity to the Duke River fault. Most events in this zone occur north of the mapped Duke River fault surface trace and the perpendicular cross section, cc', does not indicate this seismicity is occurring on a dipping fault surface. There are several areas along CC' that indicate linear features running perpendicular

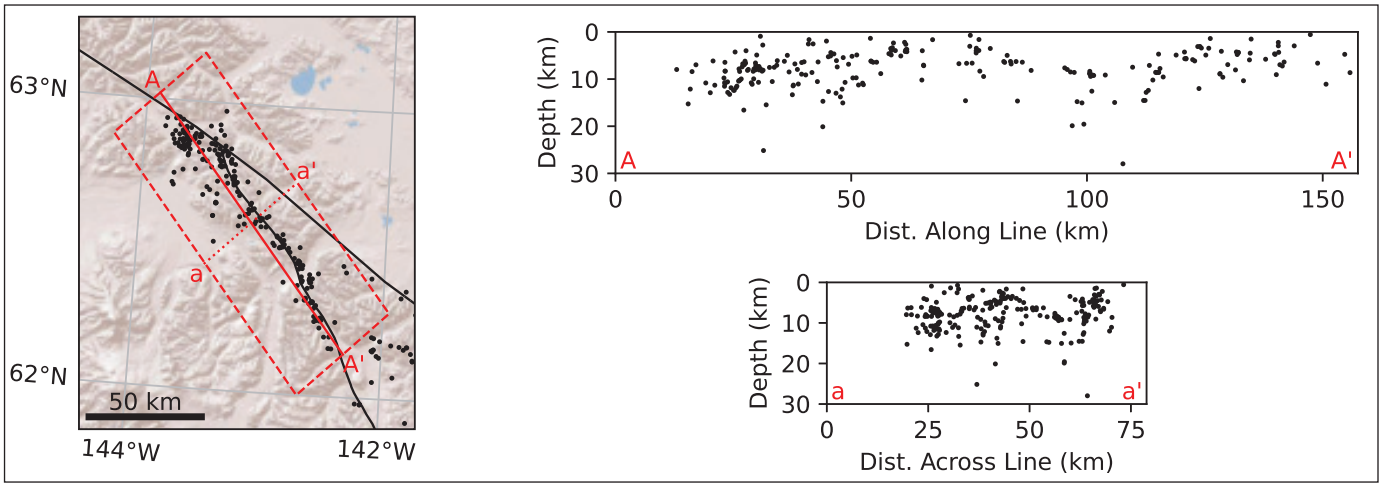

Figure 5. *Event-pair relocations for Zone AA' (in red) including map view (left), depth cross section AA' (solid line; top right), and the perpendicular cross section aa' (dotted line; bottom right). The seismicity considered along the Totschunda fault includes 239 events (dashed box).*

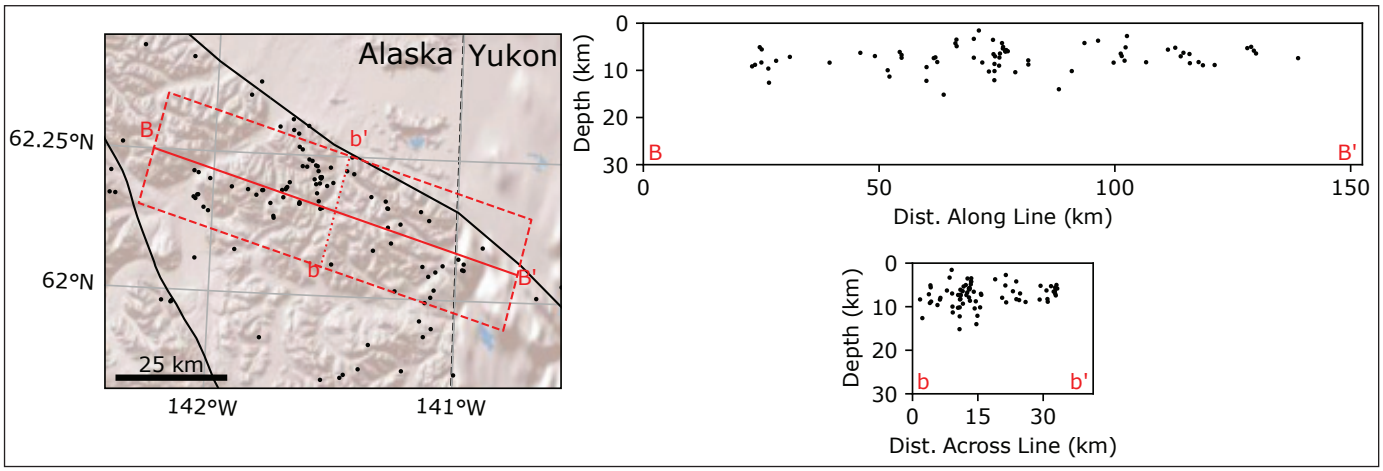

Figure 6. *Event-pair relocations for Zone BB' (in red) including map view (left), depth cross section BB' (solid line; top right) and the perpendicular cross section bb' (dotted line; bottom right). The seismicity includes 76 events (dashed box) that occur in the area between the Totschunda and Eastern Denali faults.*

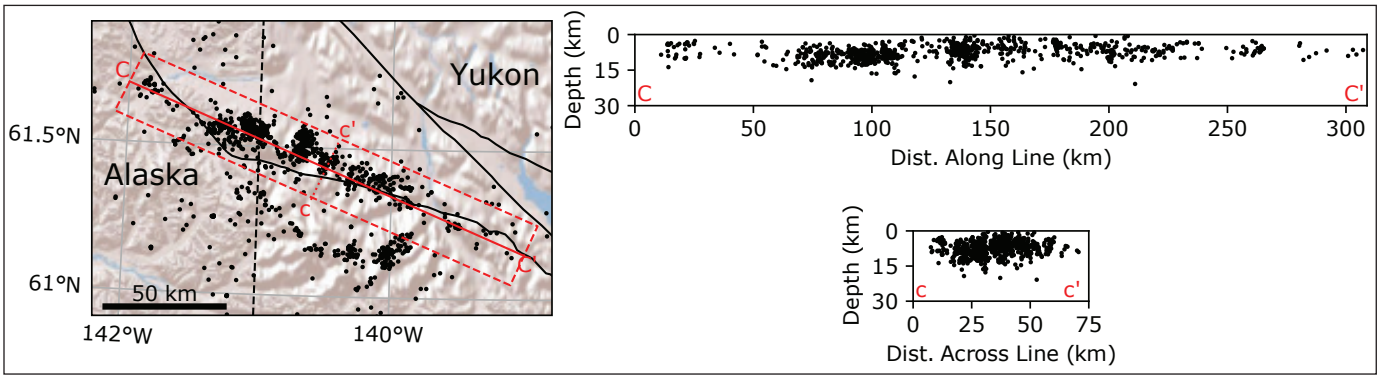

Figure 7. *Event-pair relocations for Zone CC' (in red) including map view (left), depth cross section CC' (solid line; top right) and the perpendicular cross section cc' (dotted line; bottom right). The seismicity includes 968 events (dashed box) that occur along the Duke River fault.*

to the Duke River fault system (occurring at ~90 km, ~140 km and ~160 km). For both cross sections CC' and cc', the majority of events are <15 km in depth. There are no trends in depth along either cross section. It is possible that the mapped surface feature is simply inconsistent with current seismicity or that the seismic data insufficiently constrain the absolute location of the events. The latter can be due to limitations in the velocity model employed for this location, or insufficient network coverage. Recently deployed stations by our group near Burwash Landing aim to improve resolution for similar events.

The Connector fault (Richter and Matson Jr, 1971; Lahr and Plafker, 1980) is a proposed fault connecting the Totschunda fault with the Fairweather fault system located under the St. Elias ice fields. Due to the significant ice coverage in the area, this fault has not been mapped at the surface. Slip is suggested to be up to 10 mm/yr to compensate for low slip on the Eastern Denali fault (Kalbas et *al.*, 2008). Further studies (e.g., Doser, 2014) suggest that the Connector fault is seismically active. Rupture mechanisms along this fault are mostly dextral strike-slip with some oblique components (Doser, 2014). In this study, we relocate 159 events in the geographic area of the Connector fault. These relocations indicate a clear linear feature between the Totschunda-Duke River fault system in the north and the Fairweather fault system in the south (Fig. 8). Event depths generally decrease from northwest to southeast along cross section DD'. Depths are <10 km making this the shallowest feature identified in this study.

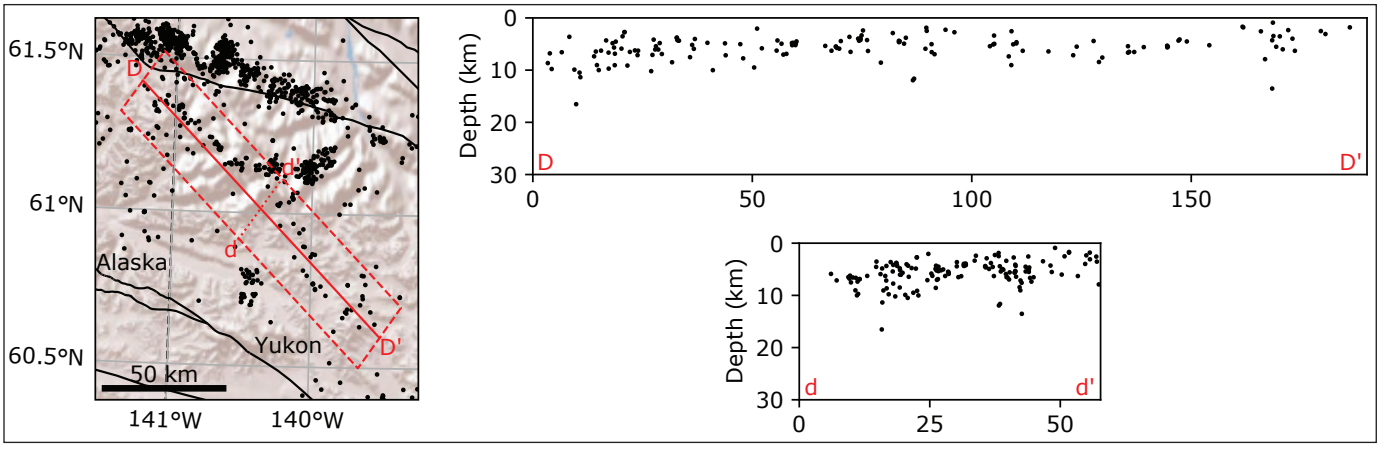

Figure 8. *Event-pair relocations for Zone DD' (in red) including map view (left), depth cross section DD' (solid line; top right) and the perpendicular cross section dd' (dotted line; bottom right). The seismicity includes 159 events (dashed box) that occur in the area of the Connector fault between the Totschunda-Duke River and Fairweather faults.*

Zone EE' (Fig. 9) is located at the southern end of Kluane Lake, and includes 135 events that start on the Duke River fault to the west and cross the surface trace of the Denali fault to the east. The seismicity does not follow the surface trace of the Denali fault, curving instead to the east along topographic lows. Event depths for this zone are interesting in both the EE' and ee' cross sections. For both EE' and ee', seismicity near the Denali fault (at ~75 km on EE' and at ~30 km on ee') is shallowest along the cross section (<8 km). Depths increase for events farther away from where the cross section crosses the Denali fault.

Zone FF' (Fig.10) includes the aftershocks of the 2017 St. Elias earthquakes (He et *al.*, 2018) with 1585 relocated events. Previous studies of this area (Choi et *al.*, 2021) have included DD relocations for portions of this aftershock sequence (1314 events) and resolved two aftershock clusters (one cluster for each of the two M 6 earthquakes). Both clusters are interpreted to be located west of the Eastern Denali fault and not directly related to it. Our relocations of the 1585 events are consistent with previous studies showing two distinct clusters: one quasi-parallel to the Eastern Denali fault and one at an angle to the Eastern Denali fault. However, there is no apparent fault dip observed on either cross sections (FF' or ff'), rather, events are densely clustered.

Travel time residuals

Figure 11 and Table 1 summarize RMS of the travel time residuals, which is modestly reduced by relocation for the overall catalogue from 1.568 to 1.501 s. The RMS of the residuals improves for Zones BB', DD', EE', and FF'. A smaller RMS means the overall residual distribution more closely matches observed data, and that we have improved absolute locations for the overall catalogue along with the events in Zones BB' (Totschunda to Denali inter-fault seismicity), DD' (Connector fault), EE' (Kluane Lake seismicity), and FF' (St. Elias sequence aftershocks). For Zones AA' and CC', the relocation RMS residuals are larger than the USGS catalogue. Therefore, we do not recover improved absolute locations for events along the Totschunda fault or along the Duke River fault. However, we do significantly improve relative cluster location precision, as event-pair residuals are reduced from 637 to 431 ms (31.8% reduction) for catalogue DTs and from 820 to 88 ms (89.6% reduction) for cross-correlation DTs.

Review of the travel time residuals both for the entire catalogue, and for each cluster, show that the widths of the residual distributions improve after relocation. Table 1 shows that for the full catalogue and for all clusters the residual standard deviation decreases after relocation.

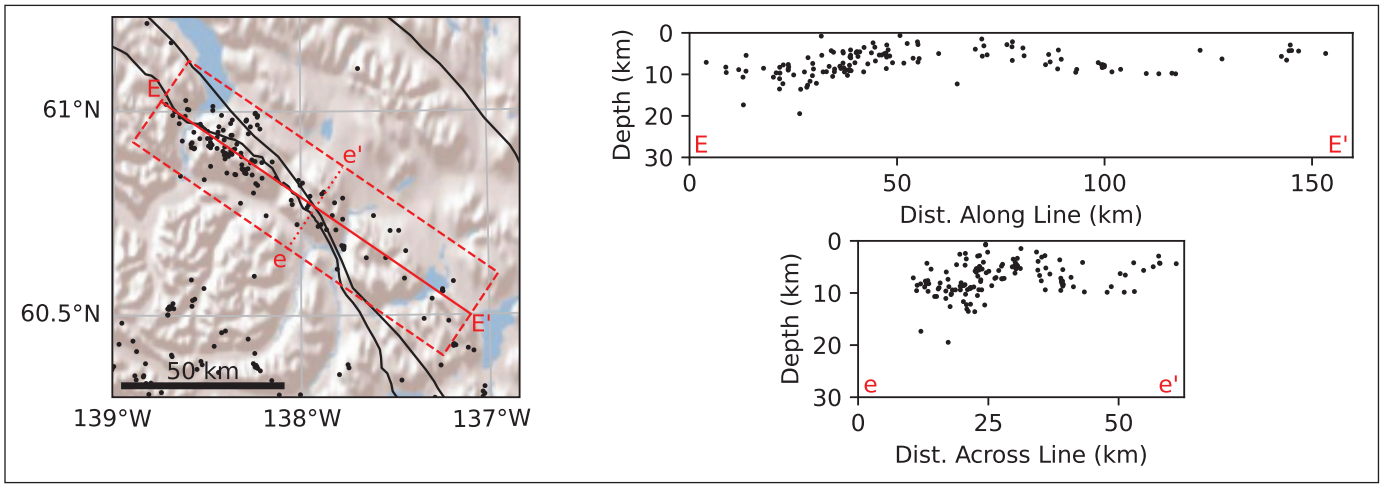

Figure 9. *Event-pair relocations for Zone EE' (in red) including map view (left), depth cross section EE' (solid line; top right) and the perpendicular cross section ee' (dotted line; bottom right). The seismicity includes 135 events (dashed box) that occur at the south end of Kluane Lake in proximity to the Duke River and Denali faults.*

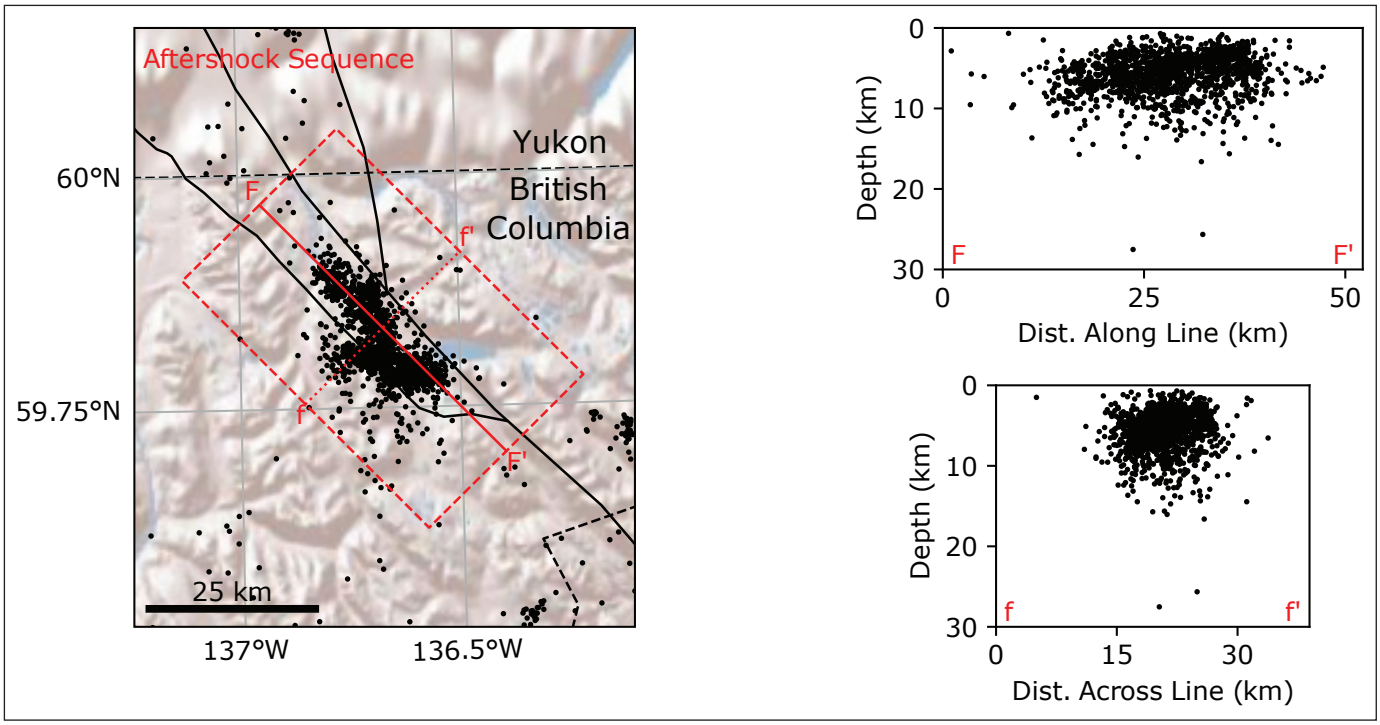

Figure 10. *Event-pair relocations for Zone FF' (in red) including map view (left), depth cross section FF' (solid line; top right) and the perpendicular cross section ff' (dotted line; bottom right). The seismicity includes 1585 events (dashed box) that are part of the aftershock sequence for the 2017 St. Elias sequence.*

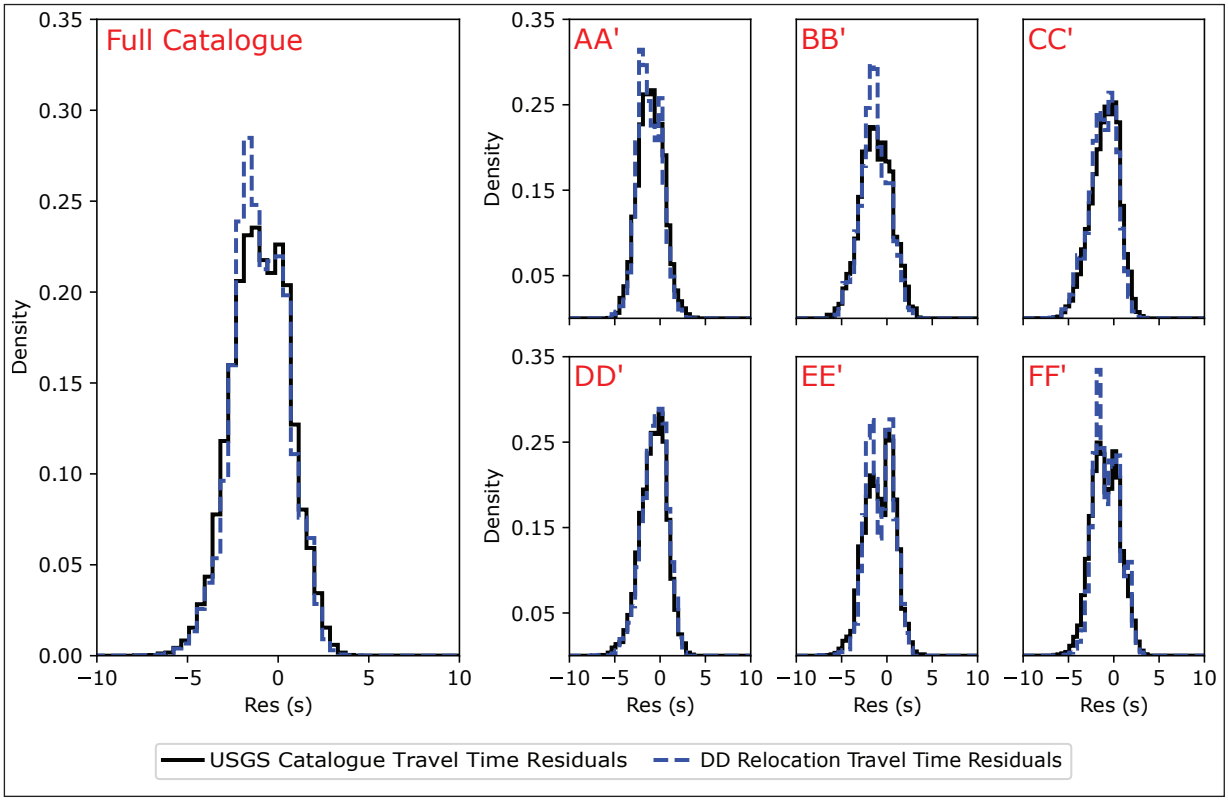

Figure 11. *Travel time residuals for starting USGS catalogue (black line) compared to travel time residuals for relocated catalogue (blue dashed line) for the full catalogue of seismic events (left) and for zones of interest AA' to FF'.*

Table 1. *Travel time residual statistics (s) for both the USGS event catalogue and the DD relocation catalogue including RMS and standard deviations for the full catalogues as well as zones of interest AA' through FF'.*

	USGS Catalogue		DD Relocation Catalogue	
	RMS Residual (s)	**Residual St. Dev. (s)**	**RMS Residual (s)**	**Residual St. Dev. (s)**
Full Catalogue	1.847	1.568	1.796	1.501
Zone AA'	1.726	1.392	1.745	1.302
Zone BB'	2.096	1.714	2.030	1.540
Zone CC'	1.845	1.566	1.956	1.535
Zone DD'	1.617	1.444	1.481	1.353
Zone EE'	1.789	1.599	1.660	1.462
Zone FF'	1.797	1.552	1.604	1.407

The travel time residuals carry a negative bias, likely due to the misfit between the velocity model (Ma and Audet, 2017) used in forward modelling and the true velocity structure. Because of the large study area, a velocity model applicable to a large region is used. Such models ignore local variations in velocity structure, which can be particularly significant in complicated tectonic settings such as the complex fault zones and mountainous regions considered here. Previous tomographic studies of the region indicate large velocity contrasts in fault zones as well as strong directional anisotropy in areas of southwestern Yukon (Schaeffer and Lebedev, 2014; Estève *et al.*, 2021). Improving the forward modelling by including such effects is a plausible but non-trivial future research objective.

Relocation uncertainty estimates

To estimate location uncertainties, we carried out 250 bootstrap iterations for several of the areas of interest. For bootstrap iterations, noisy data are resampled for relocations. Table 2 shows the median, mean and RMS location uncertainty for all spatial parameters for the relocated areas of interest. From Table 2, we see consistent uncertainties in the 1–3 km range for events in these clusters. For many events in the USGS catalogue, we have no initial uncertainty estimate for the location parameters.

Southwestern Yukon is a region of complex dextral strike-slip and oblique thrust systems. From the relocation catalogue, we propose new faults connecting the existing Totschunda-Duke River fault, Denali fault, and Fairweather fault systems and interpret the region as one regional shear zone (Fig. 12). The interpreted faults in Figure 12 include a fault in the region of Zone BB' that connects the southern end of seismicity on the Totschunda fault to the Denali fault. In addition, our results clearly show the Connector fault (Richter and Matson Jr, 1971; Lahr and Plafker, 1980) between the Totschunda-Duke River fault system and the Fairweather fault. Finally, we interpret a series of faults between the Fairweather fault and the Denali fault south of the Connector fault.

Table 2. *Median, mean and RMS uncertainties (km) for X, Y and Z location parameters for events in Zones AA', BB', DD' and EE'*

	Location Uncertainty (km)								
	Median			Mean			RMS		
	X	Y	Z	X	Y	Z	X	Y	Z
Zone AA'	1.40	1.50	1.66	2.00	2.17	2.08	2.83	3.07	2.79
Zone BB'	0.89	0.87	1.44	1.22	1.26	1.45	1.64	1.68	1.77
Zone DD'	1.39	1.31	1.11	2.04	2.02	1.61	2.87	2.93	2.19
Zone EE'	1.47	1.97	1.36	1.93	2.40	1.85	2.66	3.11	2.50

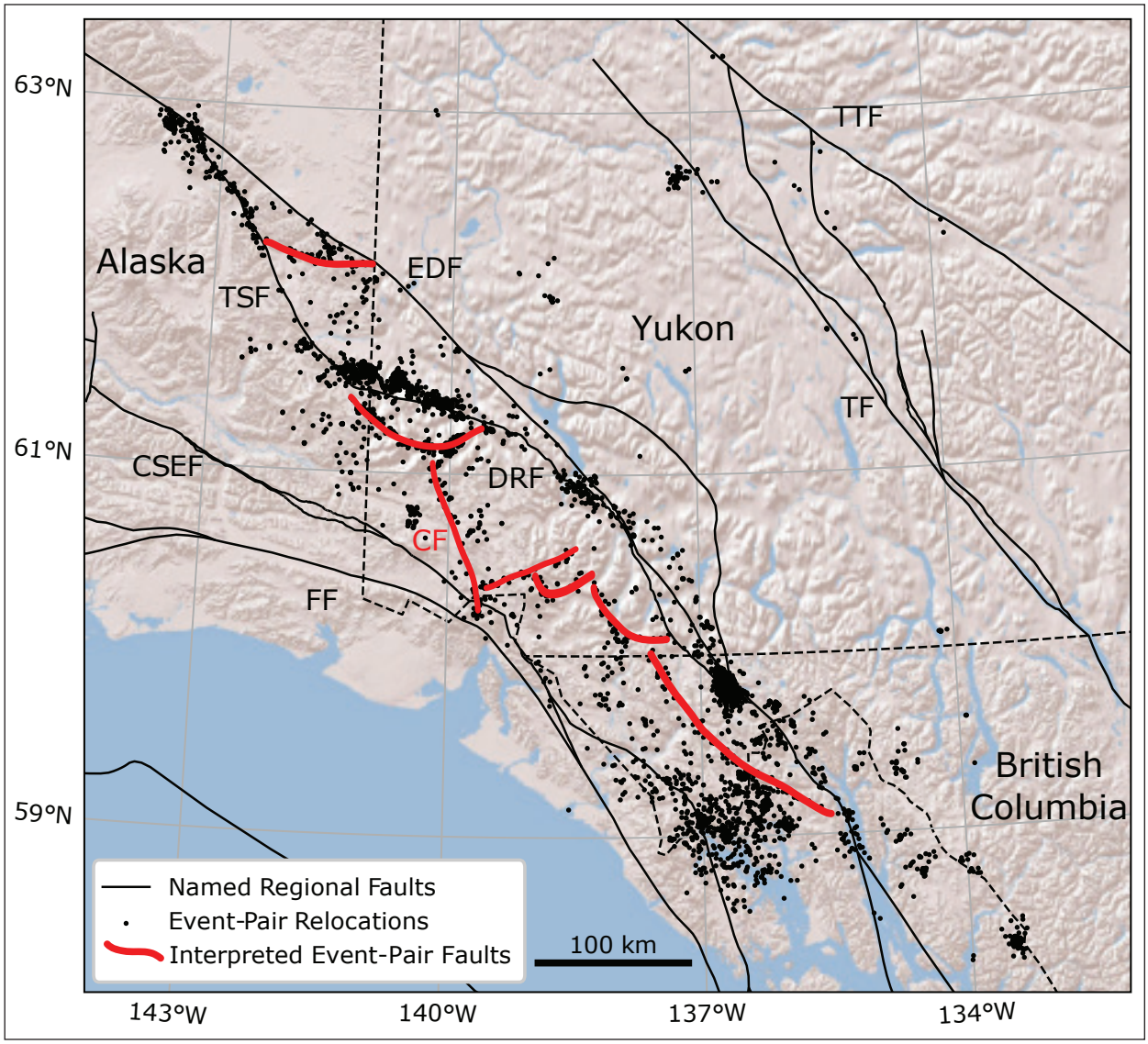

Figure 12. *Interpreted faults (red lines) identified from the event-pair relocation catalogues (black dots) plotted alongside existing named regional faults (black lines). The Connector fault (CF) is labeled in red.*

Conclusions

The DD relocation method allows for clearer images of seismicity and better precision in cluster location. In this study, we present a DD relocation catalogue of 5536 seismic events occurring between 2010 and 2021 in southwestern Yukon. We observe more precise locations of seismicity occurring in the complex dextral strike-slip systems consisting of the Totschunda, Duke River, Denali and Fairweather faults. In this location, the USGS earthquake catalogue contains significant location grid artifacts, particularly in depth, which have been removed in the DD relocation catalogue. Our relocation not only improves cluster location precision, but also improves the overall travel time residuals for the DD catalogue indicating that absolute event locations are also improved. From the relocated catalogue, we have been able to identify several new regional faults. We have identified a fault connecting the Totschunda and Denali faults at the southern end of Totschunda fault seismicity following the M 7.9 Denali earthquake. We have identified and mapped the Connector fault between the Totschunda-Duke River fault and the Fairweather fault system. We have also identified other seismically active fault features including a fault south of the Duke River fault and various faults connecting the Fairweather fault and the Denali fault to the south of the Totschunda-Duke River fault.

Acknowledgments

Funding for this research comes from the Canadian Natural Science and Engineering Research Council (NSERC), Alberta Innovates, the Society of Exploration Geophysicists (SEG), and the Yukon Geological Survey through funding from NRCan's Emerging Renewal Power Program and the Yukon government's *Our Clean Future* initiative. All seismic data are freely available through the Federation of Digital Seismograph Networks (FDSN) web services of the Incorporated Research Institutions for Seismology (IRIS; https://service.iris.edu/). The authors would like to thank the Kluane First Nation for their support of this research, Maurice Colpron for constructive feedback on this report, and David Eaton for his critical review of this work.

References

Aster, R.C., Borchers, B. and Thurber, C.H., 2018. Parameter estimation and inverse problems, Third Edition. Elsevier, https://doi.org/10.1016/C2015-0-02458-3.

Billings, S.D., 1994. Simulated annealing for earthquake location. Geophysical Journal International, vol. 118, p. 680–692, https://doi.org/10.1111/j.1365-246X.1994.tb03993.x.

Busby, R.W. and Aderhold, K., 2020. The Alaska Transportable Array: As Built. Seismological Research Letters, vol. 91, p. 3017–3027, https://doi.org/10.1785/0220200154.

Castellanos, F. and van der Baan, M., 2013. Microseismic event locations using the double-difference algorithm. CSEG Recorder, vol. 38, p. 26–37.

Choi, M., Eaton, D.W. and Enkelmann, E., 2021. Is the Eastern Denali fault still active? Geology, vol. 49, p. 662–666, https://doi.org/10.1130/G48461.1.

DeMets, C., Gordon, R.G., Argus, D.F. and Stein, S., 1990. Current plate motions. Geophysical Journal International, vol. 101, p. 425–478, https://doi.org/10.1111/j.1365-246X.1990.tb06579.x.

Dodge, D.A., Beroza, G.C. and Ellsworth, W.L., 1995. Foreshock sequence of the 1992 Landers, California, earthquake and its implications for earthquake nucleation. Journal of Geophysical Research: Solid Earth, vol. 100, p. 9865–9880, https://doi.org/10.1029/95JB00871.

Doser, D.I., 2014. Seismicity of Southwestern Yukon, Canada, and its relation to slip transfer between the Fairweather and Denali fault systems. Tectonophysics, vol. 611, p. 121–129, https://doi.org/10.1016/j.tecto.2013.11.018.

Douglas, A., 1967. Joint epicentre determination. Nature, vol. 215, p. 47–48, https://doi.org/10.1038/215047a0.

Eberhart-Phillips, D., Haeussler, P.J., Freymueller, J.T., Frankel, A.D., Rubin, C.M., Craw, P., Ratchkovski, N.A., Anderson, G., Carver, G.A., Crone, A.J., Dawson, T.E., Fletcher, H., Hansen, R., Harp, E.L., Harris, R.A., Hill, D.P., Hreinsdóttir, S., Jibson, R.W., Jones, L.M., Kayen, R., Keefer, D.K., Larsen, C.F., Moran, S.C., Personius, S.F., Plafker, G., Sherrod, B., Sieh, K., Sitar, N. and Wallace, W.K., 2003. The 2002 Denali Fault Earthquake, Alaska: A Large Magnitude, Slip-Partitioned Event. Science, vol. 300, p. 1113–1118, https://www.science.org/doi/10.1126/science.1082703.

Elliott, J.L., Larsen, C.F., Freymueller, J.T. and Motyka, R.J., 2010. Tectonic block motion and glacial isostatic adjustment in southeast Alaska and adjacent Canada constrained by GPS measurements. Journal of Geophysical Research: Solid Earth, vol. 115, https://doi.org/10.1029/2009JB007139.

Estève, C., Gosselin, J.M., Audet, P., Schaeffer, A.J., Schutt, D.L. and Aster, R.C., 2021. Surface-Wave Tomography of the Northern Canadian Cordillera Using Earthquake Rayleigh Wave Group Velocities. Journal of Geophysical Research: Solid Earth, vol. 126, https://doi.org/10.1029/2021JB021960.

Fletcher, H.J. and Freymueller, J.T., 2003. New constraints on the motion of the Fairweather fault, Alaska, from GPS observations. Geophysical Research Letters, vol. 30, https://doi.org/10.1029/2002GL016476.

Fréchet, J., 1985. Sismogenése et doublets sismiques. PhD thesis, Université Scientifique et Médicale de Grenoble, 149 p.

Geiger, L., 1910. Herdbestimmung bei Erdbeben aus den Ankunftszeiten. Nachrichten von der Gesellschaft der Wissenschaften zu Göttingen, Mathematisch-Physikalische Klasse, vol. 4, p. 331–351.

Gosselin, J., Biegel, K., Hamidbeygi, M. and Dettmer, J., 2023. Improvements in the regional earthquake focal mechanism catalogue for southwestern Yukon. In: Yukon Exploration and Geology 2022, K.E. MacFarlane (ed.), Yukon Geological Survey.

Grantz, A., 1966. Strike-slip faults in Alaska. USGS Open File Report 66-53, 82 p.

Guo, H. and Zhang, H., 2016. Development of double-pair double difference earthquake location algorithm for improving earthquake locations. Geophysical Journal International, vol. 208, p. 333–348, https://doi.org/10.1093/gji/ggw397.

Guo, H., Zhang, H., Nadeau, R.M. and Peng, Z., 2017. High-resolution deep tectonic tremor locations beneath the San Andreas Fault near Cholame, California, using the double-pair double-difference location method. Journal of Geophysical Research: Solid Earth, vol. 122, p. 3062–3075, https://doi.org/10.1002/2016JB013919.

He, X., Ni, S., Zhang, P. and Freymueller, J., 2018. The 1 May 2017 British Columbia - Alaska earthquake doublet and implication for complexity near sourthern end of Denali fault system. Geophysical Research Letters, vol. 45, p. 5937–5947, https://doi.org/10.1029/2018GL078014.

Ito, A., 1985. High resolution relative hypocenters of similar earthquakes by cross-spectral analysis method. Journal of Physics of the Earth, vol. 33, p. 279–294, https://doi.org/10.4294/jpe1952.33.279.

Kalbas, J.L., Freed, A.M. and Ridgway, K.D., 2008. Contemporary fault mechanics in southern Alaska. In: Active Tectonics and Seismic Potential of Alaska, J.T. Freymueller, P.J. Haeussler, R.L. Wesson and G. Ekström (eds.), AGU Geophysical Monograph Series 179, p. 321–336.

Lahr, J.C. and Plafker, G., 1980. Holocene Pacific–North American plate interaction in southern Alaska: Implications for the Yakataga seismic gap. Geology, vol. 8, p. 483–486, https://doi.org/10.1130/0091-7613(1980)8<483:HPAPII>2.0.CO;2.

Langevin, H., Raymond, J. and Fraser, T., 2020. Assessment of thermo-hydraulic properties of rock samples near Takhini Hot Springs, Yukon. In: Yukon Exploration and Geology 2019, K.E. MacFarlane (ed.), Yukon Geological Survey, p. 57–73.

Lanphere, M.A., 1977. Displacement history of the Denali fault system, Alaska and Canada. Canadian Journal of Earth Sciences, vol. 15, p. 817–822, https://doi.org/10.1139/e78-086.

Leonard, L.J., Mazzotti, S. and Hyndman, R.D., 2008. Deformation rates estimated from earthquakes in the northern Cordillera of Canada and eastern Alaska. Journal of Geophysical Research: Solid Earth, vol. 113, https://doi.org/10.1029/2007JB005456.

Li, C.F., Lu, Y. and Wang, J., 2017. A global reference model of Curie-point depths based on EMAG2. Scientific Reports, vol. 7.

Li, C., Peng, Z., Yao, D., Guo, H., Zhan, Z., and Zhang, H., 2018. Abundant aftershock sequence of the 2015 M w7. 5 Hindu Kush intermediate-depth earthquake. Geophysical Journal International, vol. 213, p. 1121–1134, https://doi.org/10.1093/gji/ggy016.

Lowey, G., 1998. A new estimate of the amount of displacement on the Denali fault system based on the occurrence of carbonate megaboulders in the Dezadeash Formation (Jura-Cretaceous), Yukon, and the Nutzotin Mountains sequence (Jura-Cretaceous), Alaska. Bulletin of Canadian Petroleum Geology, vol. 46, p. 379–386, https://doi.org/10.35767/gscpgbull.46.3.379.

Lundgren, P., Saucier, F., Palmer, R. and Langon, M., 1995. Alaska crustal deformation: Finite element modeling constrained by geologic and very long baseline interferometry. Journal of Geophysical Research: Solid Earth, vol. 100, p. 22033–22046, https://doi.org/10.1029/95JB00237.

Ma, S. and Audet, P., 2017. Seismic velocity model of the crust in the northern Canadian Cordillera from Rayleigh wave dispersion data. Canadian Journal of Earth Sciences, vol. 54, p. 163–172, https://doi.org/10.1139/cjes-2016-0115.

Matmon, A., Schwartz, D.P., Haeussler, P.J., Finkel, R., Lienkaemper, J.J., Stenner, H.D. and Dawson, T.E., 2006. Denali fault slip rates and Holocene–late Pleistocene kinematics of central Alaska. Geology, vol. 34, p. 645–648, https://doi.org/10.1130/G22361.1.

Meighan, L.N., Cassidy, J.F., Mazzotti, S., and Pavlis, G.L., 2013. Microseismicity and tectonics of southwest Yukon Territory, Canada, using a local dense seismic array. Bulletin of the Seismological Society of America, vol. 103, p. 3341–3346, https://doi.org/10.1785/0120130068.

Menke, W. and Schaff, D., 2004. Absolute earthquake locations with differential data. Bulletin of the Seismological Society of America, vol. 94, p. 2254–2264, https://doi.org/10.1785/0120040033.

Michelini, A. and Lomax, A., 2004. The effect of velocity structure errors on double-difference earthquake location. Geophysical Research Letters, vol. 31, https://doi.org/10.1029/2004GL019682.

Mosteller, F. and Tukey, J.W., 1977. Data analysis and linear regression. Addison-Wesley, Reading, Massachusetts.

Ogwari, P.O., DeShon, H.R. and Hornbach, M.J., 2018. The Dallas-Fort Worth airport earthquake sequence: Seismicity beyond injection period. Journal of Geophysical Research: Solid Earth, vol. 123, p. 553–563, https://doi.org/10.1002/2017JB015003.

Paige, C.C. and Saunders, M.A., 1982. LSQR: An algorithm for sparse linear equations and sparse least squares. ACM Transactions on Mathematical Software, vol. 8, p. 43–71.

Plafker, G., Hudson, T., Bruns, T. and Rubin, M., 1978. Late Quaternary offsets along the Fairweather fault and crustal plate interactions in southern Alaska. Canadian Journal of Earth Sciences, vol. 15, p. 805–816, https://doi.org/10.1139/e78-085.

Plafker, G., Moore, J.C. and Winkler, G.R., 1994. Geology of the southern Alaska margin. In: The Geology of Alaska, G. Plafker and H.C. Berg (eds.), Geological Society of America, p. 389–448.

Richter, D.H. and Matson Jr., N.A., 1971. Quaternary faulting in the eastern Alaska Range. GSA Bulletin, vol. 82, p. 1529–1540, https://doi.org/10.1130/0016-7606(1971)82[1529:QFITEA]2.0.CO;2.

Schaeffer, A.J. and Lebedev, S., 2014. Imaging the North American continent using waveform inversion of global and USArray data. Earth and Planetary Science Letters, vol. 402, p. 26–41, https://doi.org/10.1016/j.epsl.2014.05.014.

Schaff, D.P., Bokelmann, G.H.R., Beroza, G.C., Waldhauser, F. and Ellsworth, W.L., 2002. High-resolution image of Calaveras fault seismicity. Journal of Geophysical Research: Solid Earth, vol. 107, https://doi.org/10.1029/2001JB000633.

Scherbaum, F. and Wendler, J., 1986. Cross spectral analysis of Swabian Jura (SW Germany) three-component microearthquake recordings. Journal of Geophysics, vol. 60, p. 157–166.

Seitz, G.J., Haeussler, P.J., Crone, A.J., Lipovsky, P. and Schwartz, D.P., 2008. Eastern Denali fault slip rate and paleoseismic history, Kluane Lake area, Yukon Territory, Canada. In: AGU Fall Meeting 2008, San Francisco, California, abstract i.d. T53B-1947.

Share, P.-E., Castro, R.R., Vidal-Villegas, J.A., Mendoza, L. and Ben-Zion, Y., 2021. High-resolution seismic imaging of the plate boundary in northern Baja California and southern California using double-pair double-difference tomography. Earth and Planetary Science Letters, vol. 568, https://doi.org/10.1016/j.epsl.2021.117004.

Shearer, P.M., 1997. Improving local earthquake locations using the L1 norm and waveform cross correlation: Application to the Whittier Narrows, California, aftershock sequence. Journal of Geophysical Research: Solid Earth, vol. 102, p. 8269–8283, https://doi.org/10.1029/96JB03228.

VanDecar, J.C. and Crosson, R.S., 1990. Determination of teleseismic relative phase arrival times using multi-channel cross-correlation and least squares. Bulletin of the Seismological Society of America, vol. 80, p. 150–169, https://doi.org/10.1785/BSSA0800010150.

Waldhauser, F. and Ellsworth, W.L., 2000. A double-difference earthquake location algorithm: Method and application to the northern Hayward fault, California. Bulletin of the Seismological Society of America, vol. 90, p. 1353–1368, https://doi.org/10.1785/0120000006.

Waldhauser, F., Ellsworth, W.L., Schaff, D.P. and Cole, A., 2004. Streaks, multiplets, and holes: High-resolution spatio-temporal behavior of Parkfield seismicity. Geophysical Research Letters, vol. 31, https://doi.org/10.1029/2004GL020649.

Waldhauser, F. and Schaff, D.P., 2008. Large-scale relocation of two decades of Northern California seismicity using cross-correlation and double-difference methods. Journal of Geophysical Research: Solid Earth, vol. 113, https://doi.org/10.1029/2007JB005479.

Waldien, T.S., Roeske, S.M. and Benowitz, J.A., 2021. Tectonic underplating and dismemberment of the Maclaren-Kluane Schist records Late Cretaceous terrane accretion polarity and ~480 km of post-52 Ma dextral displacement on the Denali fault. Tectonics, vol. 40, https://doi.org/10.1029/2020TC006677.

Wolfe, C.J., 2002. On the mathematics of using difference operators to relocate earthquakes. Bulletin of the Seismological Society of America, vol. 92, p. 2879–2892, https://doi.org/10.1785/0120010189.

Yukon Geological Survey, 2020. A digital atlas of terranes for the northern Cordillera. Yukon Geological Survey, http://data.geology.gov.yk.ca/Compilation/2, [accessed November 2022].

Zhang, H., Nadeau, R.M. and Toksoz, M.N., 2010. Locating nonvolcanic tremors beneath the San Andreas fault using a station-pair double-difference location method. Geophysical Research Letters, vol. 37, https://doi.org/10.1029/2010GL043577.

Appendix A. Relocation catalogue

As part of this report, we have attached the DD relocation earthquake catalogue as a CSV file (Biegel_yukon_relocation.csv). The attached CSV file includes one header line with the following designations:

- EVENT ID – Event ID is the USGS origin time in the format YRMODYHRMNSEC where YR is the 4-digit integer year; MO, DY, HR, and MN are 2-digit integer codes; and SEC is the 4-digit decimal second as an integer.
- LATITUDE, LONGITUDE – These columns are the relocation latitude and longitude in decimal degree format.
- DEPTH (KM) – Depth is the relocation depth in km.
- YEAR, MONTH, DAY – The event date should be the same as the USGS event date.
- HOUR, MINUTE, SECOND – DD relocation can change the event origin time so the time columns may include a relocation time difference which leads to an updated event origin time.
- MAGNITUDE – The USGS catalogue magnitude remains unchanged during relocation.
- MEAN X UNCERTAINTY (KM), MEAN Y UNCERTAINTY (KM), MEAN DEPTH UNCERTAINTY (KM) – From the bootstrap uncertainty analysis, we have location uncertainties in km for events within Zones AA', BB', DD', and EE'. A null value in the location uncertainty means that the event belongs to one of Zones AA', BB', DD', or EE', but bootstrap did not include the event likely due to poor event pairing.
- RMS TRAVELTIME RESIDUAL (S) – For each event, we present the RMS travel time residual which is the RMS of the residual between the relocation travel times and the measured travel times from phase arrivals in the USGS catalogue. A null value for the travel time residual means that there were no phase arrivals at the stations in shown in Figure 2. These events were therefore relocated using cross-correlation differential times.